**A Unified Theory for the Interpretation of Total Pressure and Temperature in Two-Phase Flows at Subsonic and Supersonic Speeds**

Abhijit Guha

*Proceedings: Mathematical, Physical and Engineering Sciences*, Vol. 454, No. 1970 (Feb. 8, 1998), 671-695.

Stable URL:
http://links.jstor.org/sici?sici=1364-5021%2819980208%29454%3A1970%3C671%3AAUTFTI%3E2.0.CO%3B2-K

*Proceedings: Mathematical, Physical and Engineering Sciences* is currently published by The Royal Society.

Your use of the JSTOR archive indicates your acceptance of JSTOR's Terms and Conditions of Use, available at http://uk.jstor.org/about/terms.html. JSTOR's Terms and Conditions of Use provides, in part, that unless you have obtained prior permission, you may not download an entire issue of a journal or multiple copies of articles, and you may use content in the JSTOR archive only for your personal, non-commercial use.

Please contact the publisher regarding any further use of this work. Publisher contact information may be obtained at http://uk.jstor.org/journals/rsl.html.

Each copy of any part of a JSTOR transmission must contain the same copyright notice that appears on the screen or printed page of such transmission.

JSTOR is an independent not-for-profit organization dedicated to creating and preserving a digital archive of scholarly journals. For more information regarding JSTOR, please contact support@jstor.org.

http://uk.jstor.org/
Tue Apr 5 13:18:09 2005

The Royal Society

# A unified theory for the interpretation of total pressure and temperature in two-phase flows at subsonic and supersonic speeds

By Abhijit Guha†

*Department of Aerospace Engineering, University of Bristol, Queen's Building, University Walk, Bristol BS8 1TR, UK*

*Received 17 February 1997; accepted 29 May 1997*

This paper presents a unified theory on the interpretation of total pressure and total temperature in multiphase flows. The present approach applies to both vapour–droplet mixtures and solid-particle laden gases, and at subsonic as well as supersonic velocities. It is shown here that the non-equilibrium processes occurring in the vicinity of a stagnation point are important. These processes may be responsible for the generation of entropy and affect the pressure and temperature at the stagnation point. They should be properly considered while inferring, say, flow velocity or entropy generation from Pitot measurements. By proper non-dimensionalization of the relevant parameters, it is possible to find a single (theoretically obtained) calibration curve for the total pressure as a function of the particle size, which is almost independent of the constituents of the multiphase mixture and of the flow conditions. The calibration curve is a plot of a pressure recovery factor versus Stokes number and specifies the total pressure under different non-equilibrium conditions. The total pressure, predicted by the present theory, varies monotonically between the two limiting values: the frozen total pressure (when there is no interphase mass, momentum and energy transfer in the decelerating flow towards the stagnation point) and the equilibrium total pressure (when the dispersed phase, either the liquid droplets or the solid particles, is always at inertial and thermodynamic equilibrium with the continuous vapour phase). The equilibrium total pressure is always higher than the frozen total pressure. It is shown that the equilibrium total temperature, on the other hand, may be higher or lower than the frozen total temperature. In addition, unlike the case of total pressure, the calibration curve for total temperature is not so universal, and the total temperature under non-equilibrium conditions is not necessarily bounded between the frozen and equilibrium values. It is further shown that the entropy of a multiphase mixture has to be carefully interpreted and is not unequivocally related to the total pressure even in steady adiabatic flow.

**Keywords: stagnation properties; two-phase flows; Pitot tube; non-equilibrium gas dynamics; dynamics of dusty gases; entropy generation**

† The work was carried out when the author was a Fellow of Gonville & Caius College (1990–1994), Cambridge and based at Whittle Laboratory, University of Cambridge, Madingley Road, Cambridge CB3 0DY, UK.


© 1998 The Royal Society
TEX Paper

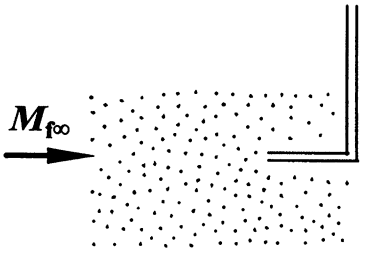


Figure 1. A Pitot tube in two-phase flow.

## 1. Introduction

A vapour–droplet flow is both scientifically interesting and of engineering importance (in a variety of areas in mechanical engineering, chemical engineering and meteorology). Applications include condensing flows of moist air or combustion products, aerosol formation in mixing processes, aerodynamic testing in cryogenic wind tunnels and wetness problems in steam turbines. Mixtures of gases laden with solid particles occur frequently in solid-propellant rocket motors and in many industrial processes.

In this paper we discuss the physics of a stagnating flow in multiphase mixtures. We also consider its engineering applications. For example, following single-phase measuring techniques, stagnation probes are often used in two-phase flow situation (e.g. Skillings 1987, 1989; Petr & Kolovratn'k 1994; Stastny & Sejna 1994; White *et al.* 1996). The question then arises: what does a total pressure or temperature probe measure when inserted in a flowing stream of such two-phase mixtures (figure 1)? The general approach of the present theory is supported by the experiments conducted by White *et al.* (1996), albeit the measurements were made in a rather limited Mach number range (see Appendix A).

The essence of the theory is that the liquid droplets or the solid particles respond to changes in temperature, velocity, etc., of the gas phase through interphase exchanges of mass, momentum and energy. These are essentially rate processes and hence significant departures from equilibrium can take place if the rate of change of external conditions, imposed by the deceleration in the stagnating flow, is comparable to the internal time scales. Thus, for example, if the size of the liquid droplets or the solid particles is very small, then inertial and thermodynamic equilibrium between the two phases are maintained always, and a Pitot tube would measure the equilibrium total pressure, $p_{0e}$. On the other hand, if the size of the droplets or the particles is very large, all interphase transfer processes remain essentially frozen. The Pitot tube records the pressure which it would have recorded if the vapour phase alone was brought to rest from the same velocity. The total pressure in this case is termed the frozen total pressure, $p_{0f}$.

As an example, consider low-pressure wet steam with a typical wetness fraction of 10% and at Mach number 1.5. Calculations show that $p_{0f}/p_\infty = 3.3$ and $p_{0e}/p_\infty = 3.79$, where $p$ is the static pressure. Therefore, in this particular example, the equilibrium total pressure is about 15% *higher* than the frozen total pressure.

For intermediate sizes of the droplets or particles, the pressure recorded by the probe would neither be the equilibrium nor the frozen value. Similar effects would also be observed regarding the measurements of stagnation temperature. Therefore, one needs some method of estimating the total pressure and temperature under non-equilibrium conditions. In spite of the theoretical interest and the practical impor-

tance of the problems, the existing literature on the former is quite modest, and that on the latter is virtually non-existent.

Taylor (1945) gave an interesting introduction to the problems of interpreting the Pitot pressure in moist air. However, no practical method was suggested for determining the true velocity from the recorded pressures. Crane & Moore (1972) improved upon the theory of Dussourd & Shapiro (1958) and presented calculations for the flow of wet steam around purged or unpurged Pitot tubes. They determined the vapour velocity field around the Pitot tube by means of an incompressible, potential flow theory and assumed that the same velocity field applies in the presence of the droplets as well. Then droplet-tracking calculations were made along different streamlines and the total droplet momentum loss was calculated within a suitable control volume. From these, the contribution of the droplets to the total pressure rise could be found. Although these calculations were quite important, Crane & Moore did not consider supersonic flows in which case a frozen shock wave stands in front of the Pitot tube. They also neglected any mass transfer between the liquid droplets and the vapour phase (which has an important effect).

In a slightly different context, some work was done on the general relaxation phenomena and the structure of shock waves in pure vapour–droplet flows (Guha 1992*a*, *b*). In particular, the flow structure in a partly dispersed shock wave is not very different from the flow structure between a frozen shock wave and the Pitot mouth. Guha's calculation methods (1992*b*) for determining the structure of partly dispersed shock waves were, therefore, extended by White *et al.* (1996) to the case of stagnating flow with a frozen shock wave. Based on these calculations, White *et al.* (1996) showed good correspondence between total pressures measured downstream of a wet-steam cascade operating with condensation shocks, and that predicted by a two-dimensional time-marching scheme. Their calculations and Pitot measurements were in the vicinity of a cascade exit Mach number 1.2 (see Appendix A).

Both Crane & Moore (1972) and White *et al.* (1996) were interested in the behaviour of wet steam, and while the former calculations are aimed for subsonic flow, the latter are restricted to supersonic flow. None of these previous authors attempted any generalization for all flow conditions and different two-phase mixtures. In this paper, calculations have been carried out for a number of two-phase mixtures—both vapour droplet and gas particle—and for a wide range of subsonic and supersonic velocities. Both Crane & Moore (1972) and White *et al.* (1996) presented the overpressure (the difference between the actual total pressure and the frozen total pressure) normalized by the upstream dynamic head (equation (4.1)). It is shown here that no generalization is possible with this non-dimensionalized parameter. Instead, a pressure recovery factor (equation (4.4)) is defined and plotted against the Stokes number. The resulting calibration curve is shown to be very general and applies (with acceptable accuracy) to all diverse two-phase mixtures studied at a wide range of flow conditions. This universal scaling law for total pressure adds to the utility of the present theory. In addition, the similar question of interpreting stagnation temperature in two-phase flows is also studied. This analysis of the stagnation temperature is believed to be the first of its kind.

## 2. Modelling a vapour–droplet mixture

A vapour–droplet medium is considered to be a homogeneous two-phase mixture of the continuous vapour phase and a large number of small liquid droplets. Surface

tension normally assures that small droplets are spherical in shape. For simplicity, a monodispersed droplet population is assumed. This means that the all the droplets are of the same size, although a prescribed size-distribution can be accommodated in a numerical calculation. The present analysis is restricted to pure substances (so that phase change is heat transfer, rather than diffusion controlled) and to low wetness fractions ($y < 0.2$) so that the volume occupied by the liquid phase is negligible. Also neglected is the partial pressure of the droplet cloud.

Sufficient number density and uniform distribution of the droplets make their interaction with the vapour describable by a continuous variation. We adopt the usual 'two-fluid' model and view the droplets as providing sources or sinks of mass, momentum and energy for the vapour, each source term varying continuously in the $x$-direction. Coagulation as well as fragmentation of droplets is neglected. Each droplet is therefore assumed to retain its identity and individual droplet radii change solely by pure evaporation or condensation.

The wetness fraction $y$ is then given by

$$y = nm, \tag{2.1}$$

where there are $n$ droplets, each of mass $m$, per unit mass of the mixture. $y$ can therefore change as a result of a change in either $n$, $m$, or both. The droplet mass, $m$, may change due to evaporation or condensation. (*Evaporation* takes place across a compression, as is the case in the decelerating flow in front of a Pitot tube.) The droplet concentration, $n$, may change as a result of velocity slip. (If there is no velocity slip between the vapour and the droplets then $n$ remains constant along a streamline.) The mass of an individual droplet is connected to its radius, $r$, and the liquid density, $\rho_\mathrm{l}$, via

$$m = \tfrac{4}{3}\pi r^3 \rho_\mathrm{l}. \tag{2.2}$$

If the vapour density is $\rho_\mathrm{g}$, the mixture density $\rho$ (neglecting the volume of the liquid phase) is

$$\rho = \rho_\mathrm{g}/(1-y), \tag{2.3}$$

and the number of droplets, $N$, per unit volume is given by

$$N = n\rho_\mathrm{g}/(1-y). \tag{2.4}$$

We assume that the vapour phase behaves as a perfect gas with constant isobaric specific heat capacity $c_\mathrm{pg}$. Thus

$$\frac{\mathrm{d}}{\mathrm{d}x}\left(\frac{p}{\rho_\mathrm{g} R T_\mathrm{g}}\right) = 0 \tag{2.5}$$

and

$$\frac{\mathrm{d}h_\mathrm{g}}{\mathrm{d}x} = c_\mathrm{pg}\frac{\mathrm{d}T_\mathrm{g}}{\mathrm{d}x}, \tag{2.6}$$

where $R$ is the specific gas constant and $T_\mathrm{g}$ is the temperature of the vapour. The perfect gas approximation is not crucial to the analysis (although this assumption is not far from reality for steam at low pressure, which is of more interest here). More realistic equations of state can be introduced if desired but these tend to complicate the algebraic development and do not provide any further physical insight.

Later we shall specify the thermal equilibrium state by the saturation temperature $T_\mathrm{s}$ rather than the pressure. The two are related by the Clausius–Clapeyron equation.

Neglecting the specific volume of the liquid and introducing the perfect gas equation for the vapour phase, we have,

$$\frac{1}{p}\frac{\mathrm{d}p}{\mathrm{d}x} = \left(\frac{h_{\mathrm{fg}}}{RT_{\mathrm{s}}}\right)\frac{1}{T_{\mathrm{s}}}\frac{\mathrm{d}T_{\mathrm{s}}}{\mathrm{d}x}, \tag{2.7}$$

where $h_{\mathrm{fg}}$ is the specific enthalpy of evaporation and is a known function of temperature.

## 3. Calculation of total pressure under non-equilibrium conditions

The analytical expressions for calculating frozen and equilibrium total pressures depend on upstream frozen Mach number, $M_{\mathrm{f}\infty}$ (equation (B 2)), and equilibrium Mach number, $M_{\mathrm{e}\infty}$ (equation (B 10)), and will be fully discussed in Appendix B. In most real situations, however, the pressure recorded by the Pitot tube will neither be the frozen nor the equilibrium value. The imposed deceleration in front of the Pitot tube would throw the vapour–droplet mixture into non-equilibrium situations, both inertially and thermodynamically. The deceleration process consequently ceases to be isentropic, as non-equilibrium exchanges of mass, momentum and energy between the two phases create entropy. The degree of the non-equilibrium effects will depend on the droplet size, mass concentration, etc., or more precisely on the relaxation times of the system. Hence, relaxation gas dynamics have to be used to obtain a solution of the problem.

For a proper solution of the real flow field around the mouth of a Pitot tube, one therefore has to solve multidimensional (at least two-dimensional axisymmetric) conservation equations with viscous, thermal and inertial non-equilibrium effects. It is important to incorporate the inertial non-equilibrium effects, i.e. to allow a velocity slip between the two phases. It is so, not only because the inertial effects are themselves significant, but also because restraining the two phases to travel at the same velocity has serious implications for the thermal equilibration process. For example, a fluid particle moving along the stagnation streamline takes infinite time to reach the stagnation point. Therefore, in the absence of any velocity slip, the vapour–droplet mixture would have time enough to come to thermal equilibrium, irrespective of the magnitude of the thermal relaxation time. In reality, however, large droplets may move without significant interphase mass and energy transfers and finally hit the inside of the probe without influencing the pressure.

Most available computational schemes (explicit time-marching, see, for example, Guha & Young (1991) and Young (1992)), however, neglect any velocity slip between the phases. In most situations with sub-micron size droplets, this is an acceptable assumption and saves computer time tremendously. (The relaxation time governing the velocity slip is very small and hence the computational time-step required for numerical simulation is small resulting in a large CPU time.) However, as explained in the previous paragraph, the effects of velocity slip cannot be neglected in a stagnating flow. Even if all these effects are incorporated in the computer programs, it is quite likely that the numerical entropy generation would make it difficult to study the desired effects (e.g. the entropy generation due to relaxation processes) properly. Hence, in this paper, we present a simple, quasi-one-dimensional model.

The basic one-dimensional gas dynamic equations for steady non-nucleating flow in a vapour–droplet system can be written in the usual way (Guha 1992*b*):

$$\text{droplet number conservation:} \quad \frac{\mathrm{d}}{\mathrm{d}x}(ANV_{\mathrm{l}}) = 0, \tag{3.1}$$

$$\text{continuity:} \quad \frac{\mathrm{d}}{\mathrm{d}x}(A\rho_{\mathrm{g}}V_{\mathrm{g}}) + \frac{\mathrm{d}}{\mathrm{d}x}(ANmV_{\mathrm{l}}) = 0, \tag{3.2}$$

$$\text{momentum:} \quad A\frac{\mathrm{d}p}{\mathrm{d}x} + \frac{\mathrm{d}}{\mathrm{d}x}(A\rho_{\mathrm{g}}V_{\mathrm{g}}^2) + \frac{\mathrm{d}}{\mathrm{d}x}(ANmV_{\mathrm{l}}^2) = 0, \tag{3.3}$$

$$\text{energy:} \quad \frac{\mathrm{d}}{\mathrm{d}x}[(h_{\mathrm{g}} + \tfrac{1}{2}V_{\mathrm{g}}^2)A\rho_{\mathrm{g}}V_{\mathrm{g}}] + \frac{\mathrm{d}}{\mathrm{d}x}[(h_{\mathrm{l}} + \tfrac{1}{2}V_{\mathrm{l}}^2)ANmV_{\mathrm{l}}] = 0, \tag{3.4}$$

where $h$ is the specific enthalpy, $V$ is the velocity, $A$ is the flow area and $x$ is the distance along the flow direction. The subscript g denotes the vapour phase and subscript l refers to the liquid properties. (Obviously equation (3.1) should be applied so long as the droplets are not evaporated completely. If complete evaporation of the liquid phase occurs in the space-marching integration of the above equations, described later in this section, before the Pitot mouth is reached, the gas dynamic equations for the pure vapour phase (equations (3.2)–(3.4) with the droplet terms removed) need to be applied for the rest of the computation.)

After considerable algebraic manipulation of equations (2.5)–(2.7) and (3.1)–(3.4), the above momentum and energy equations, (3.3)–(3.4), can be put into the form (in the same order):

$$\frac{\mathrm{d}p}{\mathrm{d}x} + \frac{p}{RT_{\mathrm{g}}}V_{\mathrm{g}}\frac{\mathrm{d}V_{\mathrm{g}}}{\mathrm{d}x} + NmV_{\mathrm{l}}\frac{\mathrm{d}V_{\mathrm{l}}}{\mathrm{d}x} - \Delta V NV_{\mathrm{l}}\frac{\mathrm{d}m}{\mathrm{d}x} = 0, \tag{3.5}$$

$$\frac{pV_{\mathrm{g}}c_{\mathrm{pg}}}{RT_{\mathrm{g}}}\frac{\mathrm{d}T_{\mathrm{g}}}{\mathrm{d}x} + NmV_{\mathrm{l}}c_{\mathrm{l}}\frac{\mathrm{d}T_{\mathrm{l}}}{\mathrm{d}x} - V_{\mathrm{g}}\frac{\mathrm{d}p}{\mathrm{d}x} = (h_{\mathrm{g}} - h_{\mathrm{l}})NV_{\mathrm{l}}\frac{\mathrm{d}m}{\mathrm{d}x} - \tfrac{1}{2}(\Delta V)^2 NV_{\mathrm{l}}\frac{\mathrm{d}m}{\mathrm{d}x} + NmV_{\mathrm{l}}\frac{\mathrm{d}V_{\mathrm{l}}}{\mathrm{d}x}, \tag{3.6}$$

where $\Delta V$ is the slip velocity given by $\Delta V = V_{\mathrm{g}} - V_{\mathrm{l}}$. Eliminating $\mathrm{d}A/\mathrm{d}x$ from (3.1) and (3.2),

$$\frac{\mathrm{d}}{\mathrm{d}x}\ln(NV_{\mathrm{l}}) = \frac{\mathrm{d}}{\mathrm{d}x}\ln(\rho_{\mathrm{g}}V_{\mathrm{g}} + NmV_{\mathrm{l}}). \tag{3.7}$$

The temperature $T_{\mathrm{l}}$ is assumed uniform throughout a droplet and always at its steady-state value, which is usually close to the saturation temperature. It is shown (Guha 1992*b*) that the time scale $\tau_{\mathrm{D}}$ with which the droplet temperature approaches this steady-state value, following a perturbation, is extremely small. Hence, although it is easy to include this relaxation process in a numerical scheme, the time-step required for stable numerical integration would be necessarily very small. It is, therefore, justifiable to neglect the droplet temperature relaxation process (without much loss in accuracy but with a large reduction in CPU time) in a practical calculation of the present nature. The upshot is that $\mathrm{d}T_{\mathrm{l}}/\mathrm{d}x$ in (3.6) can be expressed in terms of $\mathrm{d}p/\mathrm{d}x$ via equation (2.7).

The equation set (3.5)–(3.7) is incomplete and must be supplemented by two equations representing the interphase transport of mass, momentum and energy. (The droplet temperature relaxation is neglected in this study, as explained in the previous paragraph.) The interphase transfer mechanisms are quantified in terms of relaxation times which represent the time scales with which the two-phase system reverts to equilibrium following a disturbance. As non-equilibrium variables, we choose $\Delta V = V_{\mathrm{g}} - V_{\mathrm{l}}$ to represent velocity (or inertial) relaxation and $T_{\mathrm{l}} - T_{\mathrm{g}}$ to represent vapour thermal relaxation. (Note that the subcooling, $\Delta T = T_{\mathrm{s}} - T_{\mathrm{g}}$,

represents the negative of the vapour superheat.) The interphase transfer equations can be written as (Guha 1992*b*)

$$\frac{\mathrm{d}V_\mathrm{l}}{\mathrm{d}t_\mathrm{l}} = \frac{\Delta V}{\tau_\mathrm{I}}, \tag{3.8}$$

$$(h_\mathrm{g} - h_\mathrm{l})n\frac{\mathrm{d}m}{\mathrm{d}t_\mathrm{l}} = \frac{(1-y)c_{\mathrm{pg}}(T_\mathrm{l} - T_\mathrm{g})}{\tau_\mathrm{T}}, \tag{3.9}$$

where $\mathrm{d}/\mathrm{d}t_\mathrm{l} = V_\mathrm{l}\,\mathrm{d}/\mathrm{d}x$ is the substantive derivative following the droplets. The inertial relaxation time, $\tau_\mathrm{I}$, and the vapour thermal relaxation time, $\tau_\mathrm{T}$ are given by

$$\tau_\mathrm{I} = \frac{2r^2\rho_\mathrm{l}}{9\mu_\mathrm{g}}[\phi(Re) + 4.5\,Kn], \tag{3.10}$$

$$\tau_\mathrm{T} = \frac{(1-y)c_{\mathrm{pg}}\rho_\mathrm{l}r^2}{3\lambda_\mathrm{g}y}(1 + 4.5\,Kn\,/\,Pr), \tag{3.11}$$

where $\phi(Re)$ is an empirical correction for large slip Reynolds numbers ($Re = 2\rho_\mathrm{g}r|\Delta V|/\mu_\mathrm{g}$) given by

$$\phi(Re) = [1 + 0.15\,Re^{0.687}]^{-1}, \tag{3.12}$$

and $\lambda_\mathrm{g}$ and $\mu_\mathrm{g}$ are the vapour thermal conductivity and dynamic viscosity, respectively. $Pr$ is the vapour Prandtl number and $Kn = l_\mathrm{g}/2r$ is the droplet Knudsen number, $l_\mathrm{g}$ being the molecular mean free path of the vapour and $r$ the radius of the droplet. Equations (3.10) and (3.11) are supposedly valid for all droplet Knudsen numbers from the continuum to the free molecule regime. For example, for small slip Reynolds numbers and continuum flow ($Re \ll 1$, $Kn \ll 1$) equation (3.10) reduces to the Stokes drag formula for a sphere. For free molecule flow ($Kn \gg 1$) an expression derivable from kinetic theory is obtained. The expression within the bracket in equation (3.10) provides a simple interpolation formula for intermediate Knudsen numbers. Similarly, for small $Kn$, equation (3.11) reduces to the continuum expression for steady-state heat transfer from a sphere. For large $Kn$ the kinetic theory (free molecule) result is regained. The method of analysis is not dependent on the forms of (3.10)–(3.11), however, and other, possibly more suitable, expressions could easily be incorporated if desired.

When the upstream frozen Mach number is above unity, a frozen shock wave stands at a distance $X_\mathrm{s}$ from the Pitot mouth. We estimate $X_\mathrm{s}$ from the measurements given by Liepmann & Roshko (1957). These experiments show that $X_\mathrm{s}$ is proportional to the Pitot diameter (or the cross-stream height) and depends on the upstream Mach number.

The vapour velocity decreases discontinuously across the frozen shock wave which can be determined from the classical Rankine–Hugoniot equation. The variation of the vapour velocity downstream of the frozen shock is assumed to be linear. Therefore, if the velocity just downstream of the frozen shock is $V_\mathrm{gs}$, then it is assumed that

$$V_\mathrm{g} = V_\mathrm{gs}\left(\frac{X}{X_\mathrm{s}}\right), \tag{3.13}$$

where, $X$ is the distance measured from the Pitot mouth against the flow direction. When there is no frozen shock wave in the flow field (i.e. in subsonic flow), it is assumed that $V_\mathrm{g}$ varies exponentially such that

$$V_\mathrm{g} = V_\infty(1 - \exp(-X/kD)), \tag{3.14}$$

where $V_\infty$ is the unperturbed velocity far upstream, $D$ is the Pitot diameter and $k$ is an empirical constant. However, it is explained later that the non-dimensional representation of the total pressure does not depend on specific values of $k$. Equation (3.14) gives $V_g = V_\infty$ as $X \to \infty$ and $V_g = 0$ at $X = 0$.

Given (3.13) and (3.14), equations (3.5)–(3.9) represent five ordinary differential equations for five variables, $p$, $T_g$, $N$, $V_l$ and $m$. Hence, they may be numerically integrated. For this purpose, (3.5), (3.6), (3.8) and (3.9) are integrated by a fourth-order Runge–Kutta procedure. At the end of each computational step, the value of $N$ is then updated by using (3.7). (Note, from (3.7), that the wetness fraction at the stagnation point may attain a very low value in a frozen flow, in which the droplet velocity changes only slightly. This happens as a result of a negligible concentration there, although the size of each droplet hardly changes.)

A computational procedure that marches forward in space must necessarily start from an initial condition that represents a deviation from equilibrium. When $M_{f\infty} > 1$, the flow variables representing the vapour phase (e.g. $p$, $V_g$ and $T_g$) change discontinuously across the frozen shock, while the flow variables for the liquid phase ($V_l$, $N$ and $m$) remain unaltered at their respective far-upstream values. The difference in the vapour and liquid phase flow variables just downstream of the frozen shock discontinuity constitute the required initial departure from equilibrium. In subsonic flow ($M_{f\infty} < 1$), arbitrary perturbation of the flow must be specified at a sufficient distance from the Pitot mouth. The perturbation is thought to be generated by a small compression wave in the vapour phase. Step-by-step integration of the conservation equations, (3.5)–(3.9), then specifies the variation of all flow variables. Providing the initial perturbation is sufficiently small, the numerical results closely approach the exact solution.

The numerical scheme used for the present purpose is similar to that employed for the analysis of the structure of shock waves (Guha 1992*b*). All the interesting behaviour of fluid properties in a partly dispersed shock wave, as discussed in that reference, can also be observed in a stagnating flow with a frozen shock wave. (This includes, for example, the initial rise in vapour temperature downstream of the frozen shock, the many complicated pattern of the variation of wetness fraction, the initial rise in slip velocity if the frozen shock wave is weak or the case of complete evaporation.) Here we concentrate only on the pressure calculated at the stagnation point.

## 4. Results and discussion for vapour–droplet flow

Usually the results are plotted as the overpressure (the difference between the actual total pressure and the frozen total pressure), normalized by the dynamic head, versus Stokes number, $St$ (see, for example, Crane & Moore 1972; White *et al.* 1996),

$$\frac{p_0 - p_{0f}}{0.5\rho_\infty V_\infty^2} = \frac{4y_\infty}{1 - y_\infty} J(St), \tag{4.1}$$

$$St = \frac{\tau_I V_\infty}{L}, \tag{4.2}$$

where the subscript $\infty$ refers to the respective unperturbed flow variables at the far upstream. The Stokes number $St$, given by (4.2), is nothing but a Damkohler parameter signifying the importance of the relaxation processes and $L$ is a representative

Figure 2

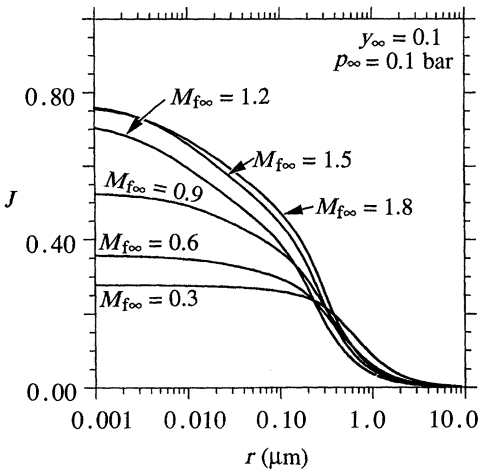


Figure 3

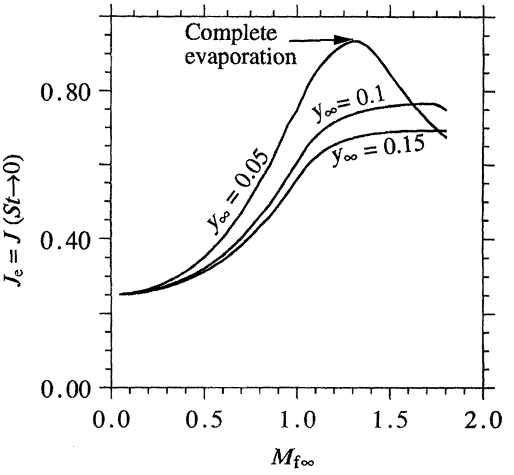


Figure 2. Variation of $J$ (defined by equation (4.1)) with droplet radius at different upstream frozen Mach numbers in wet steam.

Figure 3. Variation of equilibrium $J$ with upstream frozen Mach number for different wetness fractions (wet steam).

length scale (its appropriate value is given later in this section). If $St \to \infty$, then the internal relaxation processes are infinitely slow compared to the external time scale. Hence this represents the limiting case of frozen flow, where $p_0$ should be same as $p_{0f}$ and the value of $J$ should be zero. If $St \to 0$, then the full equilibrium flow results. Thus the function $J$ in (4.1) essentially specifies the calibration curve for a Pitot tube.

Numerical calculations are performed here for wet steam. However, the results and conclusions should also be valid for other pure vapour–droplet mixtures. Figure 2 plots the values of $J$ calculated from the present scheme against the droplet radius, covering a wide range of upstream Mach numbers. The value of $J$ indeed tends to zero for very large droplets, having large relaxation times. However, $J$ varies significantly with droplet size as well as with Mach number. Crane & Moore (1972), on the other hand, recommended a universal value of $J = 0.3$. (Their sample calculations were based on $M_{f\infty} = 0.8$.) White *et al.* (1996), however, showed the variation of $J$ with droplet sizes but concluded that it was virtually independent of the Mach numbers. This was so because White concentrated only on supersonic flow over a limited Mach number range.

It should be emphasized that the equilibrium value of $J$, as the droplet radius tends to zero, can be calculated directly from the conservation equations as discussed in Appendix B. Therefore, this limiting value ($J_e = J\ (St \to 0)$) will be independent of any non-equilibrium calculation scheme and can be calculated with certainty. Figure 3 plots this limiting value of $J_e$ as a function of upstream frozen Mach number, with the upstream wetness fraction, $y_\infty$, as the parameter. The point where the curve for $y_\infty = 0.05$ starts decreasing represents the Mach number at which the resulting deceleration is just enough to evaporate the liquid phase completely. That all the curves in the low subsonic limit tend to a unique value can be explained by combining (B 1) and (B 9) and then letting $M_{f\infty} \to 0$, which results in

$$\lim_{M_{f\infty}\to 0} \frac{p_{0e} - p_{0f}}{0.5\rho_\infty V_\infty^2} = \frac{y_\infty}{1 - y_\infty}. \tag{4.3}$$

Figure 4

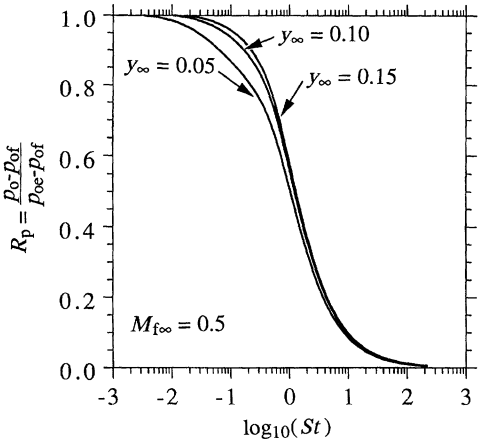


Figure 5

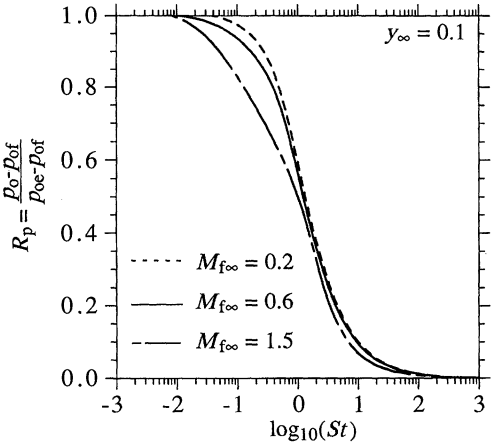


Figure 4. Variation of non-dimensionalized total pressure with Stokes number for different wetness fractions in wet steam.

Figure 5. Variation of non-dimensionalized total pressure with Stokes number for different upstream frozen Mach numbers in wet steam.

Clearly, the function $J$ is not unique for all flow conditions and, hence, not very useful as a calibration curve. It was found during the present course of research that a much better non-dimensional parameter is $R_p$, defined by

$$R_p = \frac{p_0 - p_{0f}}{p_{0e} - p_{0f}}. \tag{4.4}$$

$R_p$ may thus be physically interpreted as a pressure recovery factor. One of the advantages of using $R_p$, as opposed to $J$, is obvious. The value of $R_p$, unlike $J$, is bounded between 0 and 1 as the Stokes number varies from $\infty$ to 0. Thus the maximum error in the predicted overpressure is $p_{0e} - p_{0f}$, and the predicted total pressure *always* lies within its two limiting values. There is no such limit on the error using $J$, since the dynamic head is used to non-dimensionalize it. For example, according to figure 2, if a universal calibration curve for $J$ was adopted based on, say, $M_{f\infty} = 1.5$ and is used when $M_{f\infty} = 0.3$, the overpressure could be overpredicted by a factor of three.

Figure 4 shows the variation of $R_p$ versus Stokes number, for different wetness fractions. The effect of the wetness fraction is quite small. Figure 5 shows the influence of the upstream frozen Mach number on the calibration curve. Again, the variation is not much when it is appreciated that the present theory is based on a simple one-dimensional analysis and cannot be expected to capture all the complicated fluid mechanical phenomena. It can be seen that choosing the curve for $M_{f\infty} = 0.6$, would give quite a universal calibration of the Pitot tube for a wide range of Mach numbers. In order to appreciate the effect of the size of the Pitot tube, the diameter of the tube was varied from 0.05–10 mm. This variation would have the same effect as varying $k$ in (3.14) in the subsonic calculations, while keeping the probe diameter fixed. It was found that the *non-dimensional* calibration curve was virtually unchanged on the scale of the graphs. (It is found that the best matching, including the results presented in the next section, is obtained when the characteristic length used in (4.2) is taken as $L = kD$ in the subsonic flow, and $L = 0.5X_s$ in the supersonic case.)

*It should be noted that the denominator in the expression for $R_p$ (equation (4.4))*

*is calculated using the* equilibrium *gasdynamic calculations (hence performed with certainty) described in Appendix B, whereas the numerator is calculated using the* non-equilibrium *calculations as discussed in § 3. That the value of* $R_p$ *indeed tends to unity and zero in the appropriate limits of St (figure 4), demonstrates independent theoretical consistency of the calculation schemes.*

## 5. Total pressure in a solid-particle-laden gas

An excellent review of the dynamics of dusty gases is given by Marble (1970). He, however, did not specifically consider the question of total pressure.

An almost similar analysis for calculating the total pressure, as presented in § 4, also applies to a solid-particle-laden gas. In fact, the analysis gets somewhat simpler because a mixture of solid particles and a perfect gas, at inertial and thermodynamic equilibrium, behaves as a modified perfect gas with an isentropic exponent, $\bar{\gamma}$, given by

$$\bar{\gamma} = \frac{(1-y)c_{pg} + yc}{(1-y)(c_{pg} - R) + yc}, \tag{5.1}$$

where $c$ is the specific heat of the solid particles. (Compare $\bar{\gamma}$ with the isentropic exponent $\gamma_e$, of a vapour–droplet mixture given by (B 7).) Following (B 11), the equilibrium sonic speed is given by $a_e = \sqrt{\bar{\gamma}p/\rho}$, where $\rho$ is the mixture density. Thus the equilibrium total pressure $p_{0e}$ can be calculated from the ideal gas isentropic relations (equation (B 1) with $\bar{\gamma}$) in the subsonic case, and from the classical Rayleigh equation for the Pitot tube (again with $\bar{\gamma}$) when the flow is supersonic and a shock wave is present in front of the tube. There is no interphase mass transfer involved. Hence the sizes of the solid particles do not change and much of the complexity faced in the vapour–droplet flow calculations due to complete evaporation does not exist in a solid particle laden gas.

Equations (3.1)–(3.8) are equally applicable to a solid-particle-laden gas. The main difference between the equations for vapour–droplet and gas–particle mixtures lies in the facts that there is no interphase mass transfer in the latter case and that the pressure and temperature of a gas–particle mixture, even at equilibrium, are independent of each other. (The pressure and temperature of an equilibrium, wet vapour are, on the other hand, related by equation (2.7).) Therefore, the term $\mathrm{d}m/\mathrm{d}x$ in the above-mentioned equations is always zero, and one needs an equation describing the rate of change of the temperature of the solid particles. This is obtained by equating the thermal inertia term for the solid particles with the rate of heat transfer to a cold spherical particle from the hot surrounding gas. The resulting equations are

$$\frac{\mathrm{d}T_p}{\mathrm{d}x} = \frac{T_g - T_p}{V_p \tau_{Tp}}, \tag{5.2}$$

$$\tau_{Tp} = \frac{r^2 \rho_p c}{3\lambda_g}\left(1 + \frac{4.5\,Kn}{Pr}\right), \tag{5.3}$$

where, the subscript 'p' refers to the solid particles. The equations for velocity slip remain unaltered. (The same equations (3.8) and (3.10), with the subscript p instead of l, are valid in gas–particle mixtures.) Since the radii of the solid particles do not change, the relaxation times given by (3.10) and (5.3) remain almost constant. (On the other hand, the interphase mass transfer in a vapour–droplet mixture results in substantial changes in the relaxation times, especially close to the point of complete

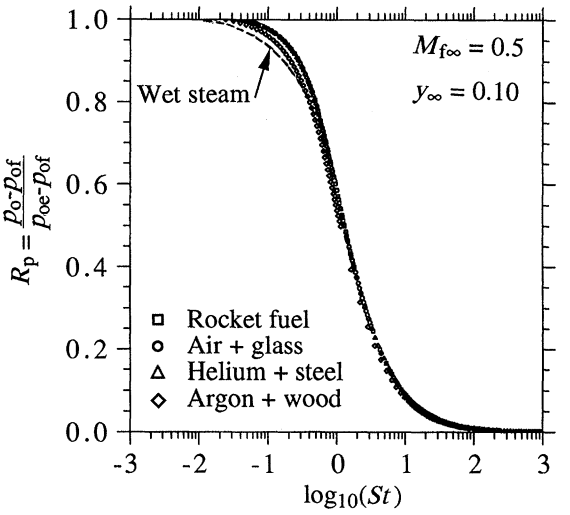


Figure 6. Variation of non-dimensionalized total pressure with Stokes number for different two-phase mixtures.

Table 1. *Property values for different gas–particle mixtures (SI units)*

| | $R$ | $\gamma$ | $c_{pg}$ | $\mu_g \times 10^5$ | $\lambda_g$ | $c$ | $\rho_p$ | $\delta = c/c_{pg}$ |
|---|---|---|---|---|---|---|---|---|
| rocket fuel | 418.8 | 1.2 | 2513 | 6.4 | 0.2737 | 1424 | 3848 | 0.57 |
| air + glass particles | 287 | 1.4 | 1004.5 | 1.85 | 0.0262 | 840 | 2720 | 0.84 |
| He + steel particles | 2039.7 | 1.65 | 5193.5 | 2 | 0.1482 | 461 | 7823 | 0.09 |
| Ar + wood dust | 208 | 1.67 | 565 | 1.37 | 0.011 | 2387 | 818 | 4.22 |

evaporation (Guha 1992*b*).) Step-by-step numerical integration of equations (3.5)–(3.8) and (5.2) then generates the pressure profile in front of the mouth of the Pitot tube.

Figure 6 shows the calculated variation of $R_p$ versus Stokes number for a number of gas–particle mixtures (all with $M_{f\infty} = 0.5$). Four different mixtures are considered to give a wide variety of different thermophysical properties—a typical mixture used in solid propellant rocket motors, air plus glass particles, Helium plus stainless steel particles and Argon plus wood dust. The property values are collected from various sources and are shown in table 1 in SI units, all at 1 bar and 293 K.

It may be seen from figure 6 that the curves for different gas–particle mixtures are almost superposed on each other. The curve for wet steam at $M_{f\infty} = 0.5$ is also included in the same figure to compare the results in gas–particle mixtures with that in a vapour–droplet flow (the calculation methods are somewhat different as explained earlier). Similar calculations were repeated for all four gas–particle mixtures at a variety of Mach numbers ($M_{f\infty}$ varying from 0.2–2) and the curves remained virtually the same (much less variation than in vapour–droplet flow, shown in figure 5). Thus it may be concluded that the $R_p$ versus $St$ curve for wet steam at $M_{f\infty} = 0.6$, as shown in figure 5, may be adopted as a universal total pressure calibration curve in two-phase flows, either of gas–particle or of vapour–droplet mixtures, at most working conditions.

## 6. Interpretation of total temperature in two-phase flows

Equations (5.3) and (3.10) may be compared to find the relative magnitudes of the thermal and inertial relaxation times in a gas–particle mixture. Their ratio in the continuum limit ($Kn \to 0$) with small slip Reynolds number reduces to

$$\tau_{\mathrm{Tp}}/\tau_{\mathrm{I}} = 1.5\delta\, Pr, \tag{6.1}$$

where $\delta$ is the ratio of the specific heat of the solid particles to that of the gas ($\delta = c/c_{\mathrm{pg}}$). Therefore, it is expected that the relative extent of the inertial and thermal relaxation zones should depend on $\delta$. Table 1 shows that $\delta$ varies between 0.09 and 4.22 for the four gas–particle mixtures considered. Yet the variation of $R_{\mathrm{p}}$ with $St$ was found to be almost independent of the constituents of the mixture (figure 6).

The variation of $\delta$, however, manifests its influence through its effects on the total temperature of the mixture. Total temperature is calculated in the present theory simultaneously with the total pressure. (Like total pressure, it is assumed that the measured total temperature is the same as the temperature of the continuous gas phase at the measuring device. The solid particles or the liquid droplets affect this temperature through interphase transfer mechanisms.) Hence, the present calculations are possibly the first analysis to throw some light on the interpretation of total temperature in two-phase flows.

It is shown in previous sections that the equilibrium total pressure is always higher than the frozen total pressure ($p_{0\mathrm{e}} > p_{0\mathrm{f}}$). The same conclusions do not apply universally in the case of total temperature. The frozen total temperature ($T_{0\mathrm{f}}$) and the equilibrium total temperature ($T_{0\mathrm{e}}$) in a *gas–particle mixture* can be found from the energy equation and are given by

$$T_{0\mathrm{f}}/T_\infty = 1 + \tfrac{1}{2}(\gamma - 1)M_{\mathrm{f}\infty}^2, \tag{6.2}$$

$$T_{0\mathrm{e}}/T_\infty = 1 + \tfrac{1}{2}(\bar{\gamma} - 1)M_{\mathrm{e}\infty}^2, \tag{6.3}$$

Taking ratios of (6.2) and (6.3), and using the definitions of $M_{\mathrm{f}\infty}$, $M_{\mathrm{e}\infty}$ (Appendix B) and $\bar{\gamma}$,

$$\frac{T_{0\mathrm{f}} - T_\infty}{T_{0\mathrm{e}} - T_\infty} = 1 + y_\infty(\delta - 1). \tag{6.4}$$

Equation (6.4) clearly shows that $T_{0\mathrm{e}}$ is higher than $T_{0\mathrm{f}}$ if $\delta < 1$, whereas $T_{0\mathrm{e}}$ is less than $T_{0\mathrm{f}}$ if $\delta > 1$. At $\delta = 1$, $T_{0\mathrm{e}} = T_{0\mathrm{f}}$. This is understood when it is realised that $\delta = 1$ implies that the mixture specific heat is the same as the specific heat of the gas alone. Therefore, in this limit, the rise in temperature is the same whether the whole mixture or the gas alone decelerates from $V_\infty$ to rest.

To see how the total temperature would depend on the particle size and other relevant parameters, a temperature recovery factor $R_{\mathrm{T}}$ is defined as follows:

$$R_{\mathrm{T}} = \frac{T_0 - T_{0\mathrm{f}}}{T_{0\mathrm{e}} - T_{0\mathrm{f}}}. \tag{6.5}$$

Figure 7 shows the variation of $R_{\mathrm{T}}$ with the Stokes number at $M_{\mathrm{f}\infty} = 0.5$, in a mixture of air and hypothetical solid particles with $\delta = 0.1$, 0.8, 1.2 and 8, respectively. It may be seen that when the value of $\delta$ is far away from unity, $R_{\mathrm{T}}$ varies monotonically from 1 to 0 as Stokes number varies from $0 \to \infty$. However, when $\delta$ is close to unity, undershooting or overshooting in the value of $R_{\mathrm{T}}$ takes place in

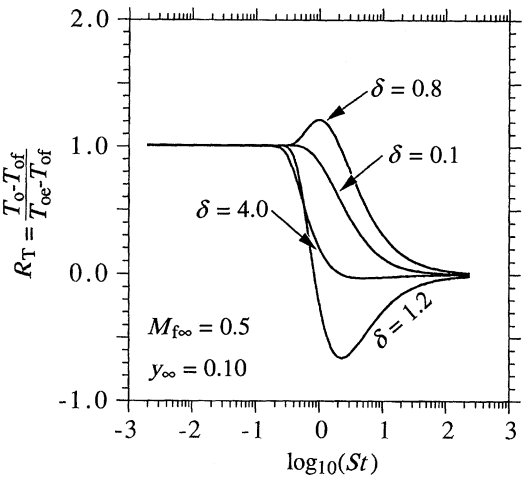


Figure 7. Variation of non-dimensionalized total temperature with Stokes number in air with solid particles of various materials.

Figure 8

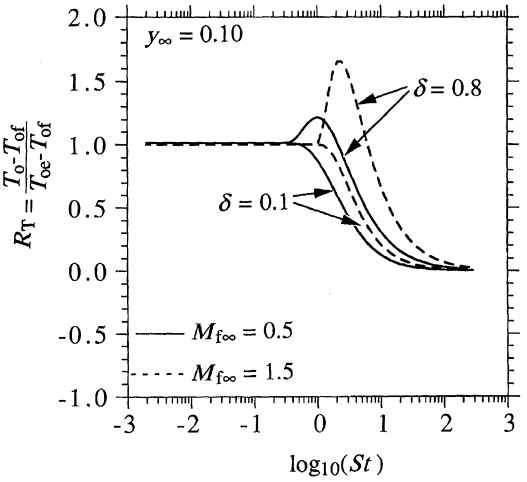


Figure 9

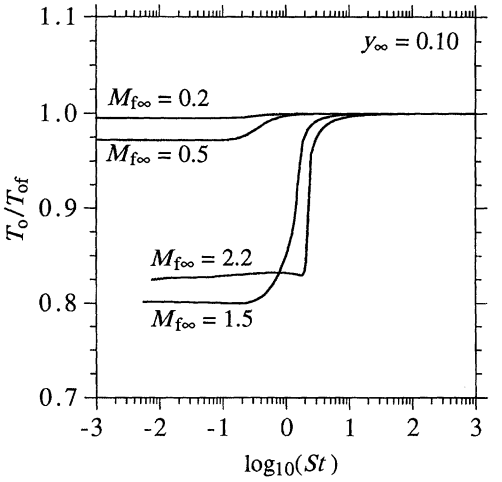


Figure 8. Effects of Mach number on the variation of non-dimensionalized total temperature with Stokes number in air with solid particles of various materials.

Figure 9. Effects of Mach number on the variation of non-dimensionalized total temperature with stokes number in wet steam.

the neighbourhood of unity Stokes number. It may be recalled that $R_p$, on the other hand, always decreases monotonically with increasing Stokes number.

Physically, the stagnation process may be appreciated by considering it in two steps. In the first step, the dissipation of the kinetic energy of the decelerating solid particles appears as internal energy of the gas phase. (This process is controlled by the relaxation time $\tau_I$.) A part of this internal energy is then transferred to the solid particles through interphase heat transfer. (This process is controlled by the relaxation time $\tau_{Tp}$.)

Figure 8 shows the effects of varying Mach number on $R_T$. The effect is quite small when $\delta$ is far away from unity. When $\delta$ is close to unity, the overshoots (and the undershoots) are quite strongly dependent on the Mach number. However, in this

case the difference in the two limiting total temperatures, $T_{0e} - T_{0f}$, itself is quite small. (Recall that $T_{0e} - T_{0f} = 0$, when $\delta = 1$. $T_{0e} - T_{0f}$ is negative when $\delta > 1$.)

The equilibrium total temperature, $T_{0e}$, in vapour–droplet flow is *always* (whether or not complete evaporation takes place) *less than* the frozen total temperature, $T_{0f}$. This may be physically explained by considering the fact that evaporation of the liquid phase takes place in a compression process. The latent enthalpy of evaporation is supplied by a reduction in the internal energy of the vapour phase, thereby reducing the temperature. Figure 9 plots the total temperature in wet steam at four different Mach numbers. The liquid phase is completely evaporated for the case $M_{f\infty} = 2.2$ ($y = 0.1$) and when the Stokes number is low. This fact has caused the total temperature to rise over the value for, say, $M_{f\infty} = 1.5$ at similar Stokes numbers.

## 7. Entropy production

As Becker (1970) points out, both frozen and equilibrium flows are *isentropic*. Relaxation effects are most pronounced when the external time scale is comparable to the internal time scale. Therefore, it is expected that the entropy production due to relaxation would be maximum when the Stokes number is of the order of unity.

In order to calculate the rise in entropy in the stagnation process, the effects of the interphase velocity slip have to be accounted for. Mixture entropy is, therefore, determined from the entropies of the individual phases by weighted averaging with their respective mass flow rates. Consider the mass flow rates at two sections, denoted by subscripts 1 and 2, along a stream tube.

$$\dot{m} = \dot{m}_{g1} + \dot{m}_{d1} = \dot{m}_{g2} + \dot{m}_{d2}, \tag{7.1}$$

where $\dot{m}$ is the total mass flow rate in the stream tube, and the subscripts g and d refer to the gas phase and the dispersed phase (liquid droplets or solid particles), respectively. If $s$, $s_g$ and $s_d$ denote the specific entropy of the mixture, the gas phase and the dispersed phase, respectively, then the rise in mixture entropy between sections 1 and 2 can be calculated from

$$s_2 - s_1 = \frac{\dot{m}_{g2}}{\dot{m}} s_{g2} - \frac{\dot{m}_{g1}}{\dot{m}} s_{g1} + \frac{\dot{m}_{d2}}{\dot{m}} s_{d2} - \frac{\dot{m}_{d1}}{\dot{m}} s_{d1}. \tag{7.2}$$

It may be noted that in the absence of velocity slip, equation (7.2) reduces to the familiar form:

$$s_2 - s_1 = (1 - y_2)s_{g2} + y_2 s_{d2} - (1 - y_1)s_{g1} - y_1 s_{d1}. \tag{7.3}$$

In a solid-particle-laden gas there is no interphase mass transfer. Therefore, the conservation of mass is separately valid for each phase ($\dot{m}_{g1} = \dot{m}_{g2}$, $\dot{m}_{d1} = \dot{m}_{d2}$). With this condition (together with the assumption that the gas phase behaves ideally), equation (7.2) takes the simpler form

$$s - s_\infty = (1 - y_\infty)\left[c_{pg} \ln\left(\frac{T_g}{T_\infty}\right) - R \ln\left(\frac{p}{p_\infty}\right)\right] + y_\infty c \ln\left(\frac{T_p}{T_\infty}\right), \tag{7.4}$$

where, $s$, $T_g$, $p$ and $T_p$ are, respectively, mixture specific entropy, gas temperature, pressure and particle temperature at any section of the stream tube, and the subscript $\infty$ refers to those values at the far upstream where the mixture is assumed to be at equilibrium. The total rise in entropy in the stagnation process can, therefore, be determined by using in equation (7.4) the numerically calculated (described in §§ 5 and 6) values of $p$, $T_g$ and $T_p$ at the Pitot mouth.

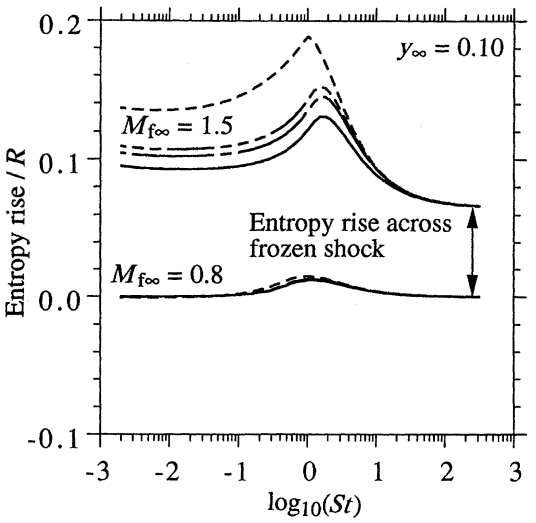


Figure 10. Entropy rise versus Stokes number in air with different solid particles: ——, $\delta = 0.1$; – – –, $\delta = 0.8$; – – – ——, $\delta = 1.2$; – – – –, $\delta = 4.0$.)

Figure 10 plots the rise in mixture entropy, as mixtures of air and solid particles are decelerated by a measuring probe from their far upstream velocity to rest. Four different solid particles (hypothetical) with $\delta = 0.1$, 0.8, 1.2 and 4 are considered and the calculations are done for two Mach numbers. For the subsonic case ($M_{f\infty} = 0.8$), figure 10 shows that the rise in entropy is indeed maximum when $St \sim 1$, and are almost zero in the frozen and equilibrium limits. (Recall from figure 6 that the total pressures are different in these limits.) When $M_{f\infty} = 1.5$, the entropy rise is again maximum close to $St \sim 1$, but it has a finite value both at $St \to 0$ as well as at $St \to \infty$. The rise in entropy in the limit $St \to \infty$ is simply that across the frozen shock. (Since the same frozen shock is involved in all the cases, this increase in entropy is the same for all four mixtures considered.) The rise in entropy in the limit $St \to 0$ is, however, different for different mixtures (it depends on $\bar{\gamma}$ and hence on $\delta$). However, it is shown by Guha (1992*a*) that if the particles come to equilibrium downstream of a frozen shock wave, then the entropy rise (across the shock plus the relaxation zone) is *not* dependent on the particle size (and hence on the relaxation times) but is determined completely by Rankine–Hugoniot equations for two-phase flow. This fact is reflected in the straight horizontal portions of the curves (at $M_{f\infty} = 1.5$) in figure 10 in the limit $St \to 0$.

The fact that the total pressure decreases monotonically from $p_{0e}$ to $p_{0f}$ as $St$ changes form 0 to $\infty$, whereas the entropy rise is zero at both limits and has a maxima when $St \sim 1$, demands care before attempting to relate a loss in total pressure with a rise in entropy.

## 8. Conclusions

A theory is presented for the calculation of total pressure and temperature in two-phase flows. The theory is based on the solution of the gas dynamic conservation equations and the interphase transfer equations. The calculations are carried out for vapour–droplet as well as gas–particle mixtures, and, at subsonic as well as supersonic speeds. The calculation scheme is robust to include the effects of complete

evaporation. (Since evaporation takes place in a stagnation process, a vapour–droplet mixture may become a single-phase dry vapour before reaching the stagnation point.) A universal scaling law for the total pressure is proposed.

It is shown that the normally used calibration parameter $J$, defined by (4.1), is *not* suitable for any generalization, and the use of $J$ may give *unbounded* large error in the estimated total pressure. The scaling law proposed here expresses a pressure recovery factor $R_p$, defined by (4.4), as a function of the Stokes number $St$, defined by (4.2). It is found that the curve for $M_{f\infty} = 0.6$ for wet steam (figure 5) can be adopted, with acceptable accuracy, as a universal calibration curve for any type of two-phase flow—vapour–droplet or gas–particle—and at any Mach number. $R_p$ varies monotonically between 1 and 0, as $St$ varies between 0 and $\infty$.

An analytical expression for calculating the equilibrium total pressure $p_{0e}$ is formulated, which is useful in finding $p_0$ if the value of $R_p$ is given. In a vapour–droplet flow, equation (B 9) gives $p_{0e}$ if complete evaporation of the liquid phase does not take place, and (B 18) in case of complete evaporation. In a solid-particle-laden gas, equation (B 9), with $\gamma_e$ replaced by $\bar{\gamma}$, always specifies $p_{0e}$.

The equilibrium total pressure is always higher than the frozen total pressure, either in a vapour–droplet or a gas–particle mixture. The equilibrium (low Stokes number solution in case of complete evaporation) total temperature in a vapour–droplet flow, on the other hand, is always less than the frozen total temperature. Equation (6.4) shows that the equilibrium total temperature $T_{0e}$ in gas–particle mixtures may be higher or lower than the frozen total temperature $T_{0f}$, depending on the magnitude of $\delta$. In addition, unlike the case of total pressure, the calibration curve for total temperature is not so universal, and the total temperature under non-equilibrium conditions is not necessarily bounded between the frozen and equilibrium values.

It is shown that the rate of entropy production in a multiphase mixture is maximum when the Stokes number is of the order unity and a reduction in measured total pressure is not unequivocally related to a rise in entropy (as it is in steady adiabatic flow of single-phase fluids). The total pressure decreases monotonically from $p_{0e}$ to $p_{0f}$ as $St$ changes from 0 to $\infty$ (figures 4–6), whereas the entropy rise is zero at both limits and has a maxima when $St \sim 1$ (figure 10). Caution must be exercised before interpreting Pitot measurements in multiphase flow.

The author is grateful to Gonville & Caius College, Cambridge, where he was a Research Fellow while conducting this work. He is also grateful to Dr J. B. Young for providing him with the computing facility.

## Appendix A.

The theory presented is plausible and testable. It is indeed hoped that the present paper would lead to new experiments suitable for direct comparison with the theory. The theory shows the quantities to measure and how to non-dimensionalize them. The experiments may, in turn, give new insight into improving certain aspects of the present theory, if required. No such elaborate data exists at the moment.

Some verification of the theory is provided by the data presented by White *et al.* (1996). Figure 19*b* from their paper is reproduced here as figure 11 for ready reference. The solid line in the figure represents the frozen total pressure calculated by a two-dimensional time-marching computational scheme which gives reasonable agreement with measurements in terms of other important quantities such as the

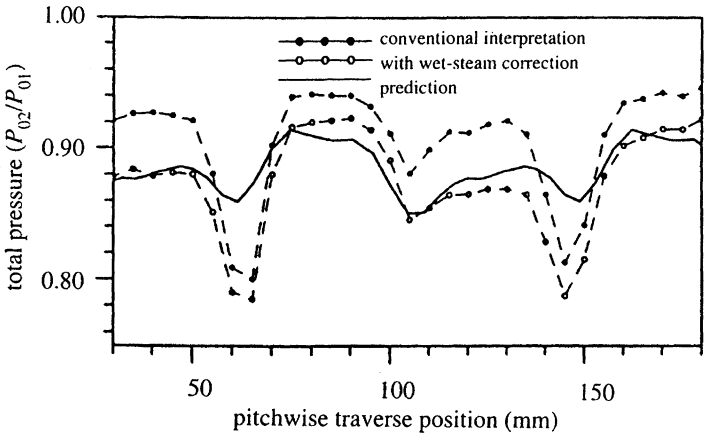


Figure 11. Comparison of measured and predicted traverse results (at the downstream location of a cascade) showing the variation of total pressure ratio. This figure is reproduced from the paper of White *et al.* (1996), their figure 19*b*.

static pressure contours. The two dotted lines represent measured total pressure—one is the raw data and the other is an interpreted value *using a non-equilibrium calculation similar to the present theory*. It is evident that the time-marching computation and conventionally interpreted Pitot measurements differ significantly and that, in the central blade passage, the theoretical and measured total pressures are in good agreement when the non-equilibrium corrections are employed. (Since the time-marching calculation scheme is an inviscid one, good agreement is not expected inside the wake region where the viscous loss is significant.) Both the calculations and the measurements were for a cascade exit Mach number of around 1.2.

Figure 12 shows the comparison of the calculations presented by White *et al.* (1996) and that predicted by the present theory for similar flow conditions. The figure depicts the variation of calculated total pressure with size of droplets in wet steam with 10% wetness fraction and an unperturbed upstream Mach number 1.24. The variables plotted as abscissa and ordinate are as chosen by White *et al.* The two predictions are similar (this is not surprising as both calculations are based on that of Guha 1992*b*). The calculations of White *et al.*, however, suggested that the variation of $J$ with droplet size was virtually independent of the Mach numbers or upstream wetness fraction. This was so perhaps because they concentrated only on supersonic flow over a limited Mach number range. Figures 2 and 3, shown in § 4 of the present paper, on the other hand, depict the very substantial variation in $J$ that is possible.

Figure 13 shows the comparison of the calculations by Crane & Moore (1972) and the present theory. The abscissa and ordinate are as chosen by Crane & Moore and the flow is subsonic (Mach number 0.8). The comparison is not very good. The Crane & Moore prediction gives almost a constant value of $J$ at 0.32, and does not either tend to the equilibrium value for very small size of the droplets or to the frozen value for very large droplets. On close inspection it is further found that, although always close to about 0.32, $J$ shows a small maxima at some intermediate Stokes number. Crane & Moore do not offer any physical explanation for these behaviours.

As explained earlier, the response time of the droplets is controlled by the relaxation times which decrease monotonically with decreasing droplet size. Thus when the droplets are very large (and consequently the relaxation time is very large) there

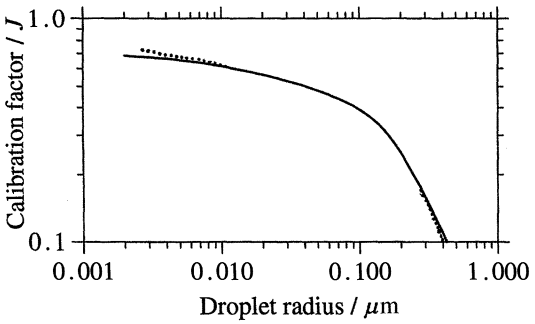


Figure 12. Variation of calibration factor $J$ with droplet radius: comparison of present theory (——) with calculations of White *et al.* (1996) (· · · · · ·). For both calculations: wet steam mixture, $M_{f\infty} = 1.24$, $y_\infty = 0.1$, $p_\infty = 16\,300$ N m$^{-2}$.

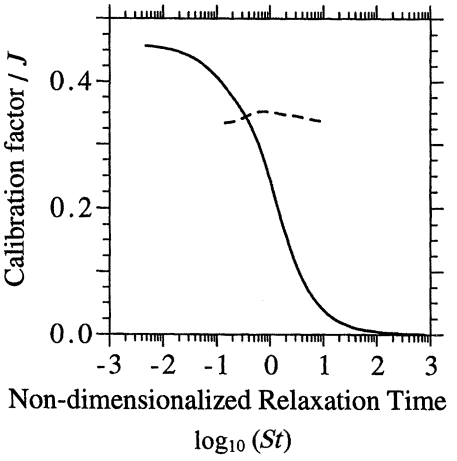


Figure 13. Variation of calibration factor $J$ with Stokes number $St$: comparison of present theory (——) with calculations of Crane & Moore (1972) (– – –). For both calculations: wet steam mixture, $M_{f\infty} = 0.8$, $y_\infty = 0.1$, $p_\infty = 0.07$ bar.

is not sufficient time for the droplets to respond to the decelerating vapour field. Thus only the vapour momentum is converted into pressure at a stagnation point. As the droplet size decreases, the contribution from decreasing droplet momentum rises and thus the total pressure increases. For very small droplets, which are capable of maintaining equilibrium with the vapour, both the vapour and the droplets come to rest at the stagnation point. This gives rise to the maximum pressure—the equilibrium total pressure. The calculations of the present theory are consistent with this physical picture.

The calculations of both Crane & Moore (1972) and White *et al.* (1996) are for wet steam. The scope of the present theory is more general—it applies to vapour–droplet flow as well as solid-particle-laden gas flow (the interphase transport of mass, momentum and energy are quite different in these two types of mixtures as explained in §§ 3 and 5). Crane & Moore calculated the vapour velocity field by potential theory (with some approximate method for including density changes) and their calculations do not apply to supersonic flow. They considered only momentum transfer between the two phases and neglected interphase mass and energy transfers which are too important to be ignored. The calculations of White *et al.*, on the other hand, are only for supersonic flow of wet steam. The present theory is applicable for subsonic as well

as supersonic flow (the gas flow field in front of the stagnation point is quite different in these two flow situations—there is a shock wave in front of a measuring device in supersonic flow). It is also shown in § 4 that neither Crane & Moore's representation ($J$ versus $St$) nor the representation of White *et al.* ($J$ versus $r$) is amenable to any generalization. The present theory, on the other hand, is formulated with a universal scaling law ($R_p$ versus $St$) such that, within acceptable accuracy, a single curve of $R_p$ versus $St$ can be proposed that can be used for any two-phase mixtures and under any flow conditions. This aspect of the present theory adds to its utility. Moreover, the present theory as its integral part also presents an interpretation of total temperature in two-phase mixtures, simultaneously with total pressure. This aspect of the theory is novel.

To sum up, the present theory for determining total pressure under non-equilibrium conditions applies to diverse two-phase mixtures (vapour–droplet or gas–particle), to various flow conditions (subsonic or supersonic) and to a wide size range of droplets or particles; the present theory proposes a universal scaling law for total pressure by carefully choosing the non-dimensional variables, and includes as an integral part of the analysis an interpretation of the total temperature.

In steady adiabatic flow of a single-phase fluid, a change in stagnation pressure is unequivocally related to a change in entropy. It is therefore common practice to measure stagnation pressure, say, upstream and downstream of a blade passage, and directly determine the amount of 'loss' or entropy generated within the blade passage (there is no 'entropy meter'). The present paper shows that this unambiguous relation between stagnation pressure and entropy does not hold in multiphase flow, and measured stagnation properties must be interpreted considering the various non-equilibrium processes taking place in the vicinity of a stagnation point.

On the quantitative aspect of the theory, it should be noted that the numerator of the pressure recovery factor, $R_p$ (equation (4.4)), that represents total pressure and is plotted in figures 4–6, is calculated from the present *non-equilibrium* theory, but the denominator is calculated from *equilibrium* thermodynamics which is certain. That the value of calculated $R_p$ indeed tends, as expected, to unity and zero in the limits of very low and very high Stokes number (representing particle size), shows independent theoretical consistency of the calculation schemes. $p_0$ can only vary between $p_{0f}$ and $p_{0e}$ according to the present theory, whereas the use of $J$ in previous works is vulnerable to large unbounded error (see § 4).

## Appendix B. Calculation of limiting total pressures in vapour-droplet flow

### (*a*) *When there is no frozen shock wave in front of the Pitot tube*

It is possible to define two limiting total pressures depending on how the vapour is brought to rest. For example, the vapour may reach the stagnation point *isentropically* while the droplets continue to move with the undisturbed upstream velocity. (The droplets would ultimately hit the inside of the Pitot tube and give rise to an axial force. But the interphase transfer of mass, momentum and energy between the two phases—the vapour and the droplets, is assumed to be absent. Hence the motion of the droplets does not contribute to the total pressure.) The total pressure recorded by the Pitot tube under these conditions will be termed as the *frozen total pressure*, $p_{0f}$. On the other hand, if the vapour is brought to rest such that, at each location in the stagnating flow, equilibrium is maintained between the two phases, the pressure

recorded by the total pressure probe will be termed as the *equilibrium total pressure*, $p_{0e}$. Note that both these processes are isentropic but result in different total pressures.

The frozen total pressure is easily calculated from the expression given in classical gas dynamics

$$\frac{p_{0f}}{p_\infty} = [1 + \tfrac{1}{2}(\gamma - 1)M_{f\infty}^2]^{\gamma/(\gamma-1)}, \tag{B 1}$$

where $\gamma$ is the isentropic exponent of the vapour phase *alone* and $M_{f\infty}$ is the frozen Mach number of the undisturbed flow. (The subscript $\infty$ is used in this paper to denote the undisturbed flow far upstream of the probe, where it is assumed that the two-phase mixture is at inertial and thermal equilibrium. The subscript 0 is used to denote stagnation quantities. The subscripts f and e are used to denote frozen and equilibrium conditions, respectively.) If $V_\infty$ is the common velocity of the vapour–droplet mixture far upstream, $M_{f\infty}$ can be calculated as

$$M_{f\infty} = V_\infty / a_{f\infty}, \tag{B 2}$$

where, $a_{f\infty}$ is the frozen speed of sound and is given by

$$a_f = (\gamma p/\rho_g)^{1/2}. \tag{B 3}$$

In order to calculate the equilibrium total pressure, $p_{0e}$, one has to write the momentum and the energy equations for the two-phase mixture (which is always at inertial and thermal equilibrium)

$$V\,\mathrm{d}V + \mathrm{d}p/\rho = 0, \tag{B 4 a}$$

$$\mathrm{d}h + V\,\mathrm{d}V = [(1-y)c_{pg} + yc_l]\,\mathrm{d}T_s - h_{fg}\,\mathrm{d}y + V\,\mathrm{d}V = 0, \tag{B 4 b}$$

where, $c_l$ is specific heat of the liquid phase, $h$ is the mixture specific enthalpy and $\rho$ is the mixture density calculated from equation (2.3). $\mathrm{d}T_s$ in equation (B 4 *b*) can be related to $\mathrm{d}p$ via equation (2.7). It can be easily verified that equations (B 4 *a*) and (B 4 *b*) are specialized forms of equations (3.5) and (3.6), in the limits $V_g \to V_l$ and $T_g \to T_l$ .

Equations (B 4 *a*) and (B 4 *b*) imply no increase in entropy due to viscous dissipation and thermal conduction. Because of the assumption of the same velocity and temperature of the two phases, there is also no rise in entropy due to relaxation processes. Equations (B 4 *a*) and (B 4 *b*) together, therefore, describe an isentropic process (represented by a vertical line in the two-phase region of a Mollier diagram). (An alternative way of looking at it would be as follows. The thermodynamic relation $T\,\mathrm{d}s = \mathrm{d}h - \mathrm{d}p/\rho$ is *separately* valid for *each* constituent phase, but, in general, is not valid for a two-phase mixture. However, the relation holds for the mixture if it is at inertial and thermal equilibrium. Equations (B 4 *a*) and (B 4 *b*) give $\mathrm{d}h = \mathrm{d}p/\rho$. Therefore, $\mathrm{d}s = 0$. In a non-equilibrium context, it can be shown that the rate of entropy production, $\Delta\dot{s}$, due to thermal relaxation is proportional to $\Delta T^2/\tau_T$, where $\Delta T$ is the interphase temperature difference and $\tau_T$ is the thermal relaxation time (Guha 1992*a*). $\Delta\dot{s} \sim \Delta T^2/\tau_T$, or, from equation (3.9), $\Delta\dot{s} \sim \dot{M}\Delta T$, where $\dot{M}$ is the rate of interphase mass transfer. For small droplets, both $\Delta T$ and $\tau_T$ tend to zero, their ratio remaining finite. The entropy generation, therefore, tends to zero as the non-equilibrium variables, e.g. $\Delta T$, tend to zero. This is why the low Stokes number non-equilibrium solution, presented in figure 4, gives the same total pressure as $p_{0e}$.)

For any assumed velocity distribution, (B 4 *a*) and (B 4 *b*) can be numerically integrated as $V$ changes from $V_\infty$ to zero. If the step size is small, the final calculated total pressure does not depend on the assumed velocity variation.

The above method of calculating $p_{0e}$ is numerical in nature, although exact. *Approximate* methods can, however, be devised to calculate $p_{0e}$ *analytically*. (Such analytical methods cannot be found in the literature.) It has been shown by Guha (1992*a*) that the pressure–density relation and the energy equation for an *isentropic* process in a pure vapour–droplet flow are approximately given by

$$p/\rho^{\gamma_e} = p_\infty/p_\infty^{\gamma_e}, \tag{B 5}$$

$$\frac{\gamma_e}{\gamma_e - 1}\frac{p}{\rho} + \tfrac{1}{2}V^2 = \frac{\gamma_e}{\gamma_e - 1}\frac{p_\infty}{\rho_\infty} + \tfrac{1}{2}V_\infty^2, \tag{B 6}$$

where the equilibrium isentropic exponent of the mixture $\gamma_e$ is given by

$$\gamma_e = \left(1 - \frac{2RT_s}{h_{fg}} + \frac{\bar{c}T_s}{h_{fg}}\frac{RT_s}{h_{fg}}\right)^{-1}, \tag{B 7}$$

where

$$\bar{c} = c_{pg} + yc_l/(1 - y). \tag{B 8}$$

The value of $\gamma_e$ is, in general, less than $\gamma$, the isentropic exponent for the vapour phase alone. For low-pressure steam, $\gamma \sim 1.32$ and $\gamma_e \sim 1.12$. While deriving equations (B 5) and (B 6) it was assumed that $\gamma_e$ remains approximately constant during the process.

By combining equations (B 5)–(B 7), it is easy to show that

$$\frac{p_{0e}}{p_\infty} = [1 + \tfrac{1}{2}(\gamma_e - 1)M_{e\infty}^2]^{\gamma_e/(\gamma_e - 1)}, \tag{B 9}$$

where the equilibrium Mach number far upstream, $M_{e\infty}$, can be calculated as

$$M_{e\infty} = V_\infty/a_{e\infty}, \tag{B 10}$$

where $a_{e\infty}$ is the equilibrium speed of sound far upstream and is given by

$$a_e = (\gamma_e p/\rho)^{1/2} = (\gamma_e(1 - y)RT_s)^{1/2}. \tag{B 11}$$

The accuracy of $p_{0e}$ calculated from equation (B 9) is obviously dependent on the acceptability of the assumption of the constancy of $\gamma_e$. A further restriction for the use of (B 6) and hence of (B 9), is that complete evaporation of the liquid phase does *not* take place during the process of stagnation. In the absence of any liquid phase, the vapour is not restrained to follow the saturation temperature, and hence a different strategy for calculating the stagnation pressure is to be followed.

We therefore need to determine the condition for complete evaporation. Combination of equations (2.3), (2.5) and (2.7) results in a relation between the differential changes of pressure, mixture density and the wetness fraction. Integration of this relation gives

$$\gamma' \ln\left(\frac{p}{p_\infty}\right) - \ln\left(\frac{\rho}{\rho_\infty}\right) = \ln\left(\frac{1 - y}{1 - y_\infty}\right), \tag{B 12}$$

where

$$\gamma' = 1 - RT_s/h_{fg}. \tag{B 13}$$

Substitution of equation (B 5) and of the condition $y = 0$ in (B 12) gives the pressure achieved at the point of complete evaporation, $p_0'$:

$$p_0'/p_\infty = (1 - y_\infty)^{-\gamma_e/(\gamma_e\gamma' - 1)}. \tag{B 14}$$

If the value of $p_{0e}$ calculated from equation (B 9) is, say, $p_0''$, and $p_0'' > p_0'$, then obviously complete evaporation takes place during stagnation. In this case the equilibrium total pressure is to be calculated in two stages. It may be assumed that, at first, the pressure rises to $p_0'$ given by (B 14) as the *equilibrium* mixture decelerates. The velocity of the vapour, $V_g'$, at the end of this phase of deceleration is given very simply from the energy equation

$$V_g' = [2(c_{pg}(T_{s\infty} - T_s') - y_\infty h_{fg} + 0.5V_\infty^2]^{1/2}, \tag{B 15}$$

where $T_s'$ is the saturation temperature at $p_0'$. The subsequent deceleration of the vapour from $V_g'$ to the stagnation point takes place under frozen conditions. Hence, the final total pressure is given by

$$\frac{p_{0e}}{p_0'} = [1 + \tfrac{1}{2}(\gamma - 1)M_{f'}^2]^{\gamma/(\gamma-1)}, \tag{B 16}$$

where $M_{f'}$ is given by

$$M_{f'} = V_g'/\sqrt{\gamma R T_s'}. \tag{B 17}$$

Combining (B 14) and (B 16),

$$\frac{p_{0e}}{p_\infty} = (1 - y_\infty)^{-\gamma_e/(\gamma_e\gamma' - 1)}[1 + \tfrac{1}{2}(\gamma - 1)M_{f'}^2]^{\gamma/(\gamma-1)}. \tag{B 18}$$

To sum up, the exact value of the equilibrium total pressure can be calculated by numerically integrating equations (B 4 *a*) and (B 4 *b*). An approximate but analytical expression for the equilibrium total pressure is given by (B 9) when complete evaporation of the liquid phase does not take place, and by (B 18) in case of complete evaporation. Calculations show that the error in using the approximate equations is less than 1% even when the upstream Mach number $M_{f\infty}$ is close to unity.

### (*b*) *When there is a frozen shock wave in front of the Pitot tube*

If the upstream frozen Mach number $M_{f\infty}$ is greater than one, then a frozen shock wave forms in front of the Pitot tube. Methods of calculation for the frozen total pressure in this case are exactly same as in a single-phase ideal gas. The pressure and velocity just after the frozen shock are calculated using the classical Rankine–Hugoniot relations. Subsequent deceleration to rest is calculated using isentropic relations. There is a loss in stagnation pressure and a rise in entropy because of the presence of the shock wave.

The equilibrium total pressure can be calculated approximately in a similar manner. It is assumed that, following disruption by the frozen shock wave, the vapour–droplet mixture comes to equilibrium, and then this equilibrium mixture undergoes further deceleration up to the stagnation point. This latter phase of deceleration is isentropic. The rise in pressure across the equilibrium shock wave can be calculated from the two-phase Rankine–Hugoniot relations given by Guha (1992*a*), whereas the further rise in pressure due to isentropic deceleration up to the stagnation point may be calculated using the theory presented in Appendix B *a*. It has been shown (Guha 1992*a*) that the pressure and velocity ratio across a partly dispersed shock wave in a vapour–droplet medium is given by

$$\frac{p_s}{p_\infty} = \frac{2\gamma_e}{\gamma_e + 1}M_{e\infty}^2 - \frac{\gamma_e - 1}{\gamma_e + 1}, \tag{B 19}$$

$$\frac{V_s}{V_\infty} = \frac{(\gamma_e - 1)M_{e\infty}^2 + 2}{(\gamma_e + 1)M_{e\infty}^2}, \tag{B 20}$$

where the subscript s is used to denote properties just downstream of the partly dispersed shock wave and the subscript $\infty$ is used, as previously, for far upstream conditions. At point s, the vapour–droplet mixture is at equilibrium and $V_s$ calculated from (B 20) is subsonic. Hence, the methods described in Appendix B *a* can be used to determine the further rise in pressure as the mixture decelerates from velocity $V_s$ to rest. Note that equations (B 19) and (B 20) are valid if complete evaporation of the liquid phase does not take place *within* the dispersed shock wave itself. If, however, this does take place then alternative equations for jump conditions, given again by Guha (1992*a*), have to be used.

## Nomenclature

| | |
|---|---|
| $a$ | speed of sound |
| $c$ | specific heat of solid |
| $c_p$ | specific heat at constant pressure |
| $h$ | specific enthalpy |
| $h_{fg}$ | specific enthalpy of evaporation |
| $J$ | calibration factor (equation (4.1)) |
| $M$ | Mach number |
| $m$ | mass of a droplet or particle |
| $\dot{m}$ | mass flow rate |
| $N$ | number of droplets (or particles) in unit volume of mixture |
| $n$ | number of droplets (or particles) in unit mass of mixture |
| $p$ | pressure |
| $p_0$ | total pressure |
| $Pr$ | Prandtl number |
| $R$ | specific gas constant of vapour |
| $r$ | radius of droplets or particles |
| $R_p$ | pressure recovery factor (equation (4.4)) |
| $R_T$ | temperature recovery factor (equation (6.5)) |
| $s$ | specific entropy |
| $St$ | Stokes number (equation (4.2)). Low and high $St$ correspond to small and large $r$, respectively |
| $T$ | temperature |
| $T_0$ | total temperature |
| $T_s$ | saturation temperature |
| $V$ | velocity |
| $x$ | flow co-ordinate |
| $y$ | mass fraction of dispersed phase |
| $\gamma$ | isentropic index of vapour phase |
| $\bar{\gamma}$ | equilibrium isentropic index in gas–particle mixture (equation (5.1)) |
| $\gamma_e$ | equilibrium isentropic index in vapour–droplet mixture (equation (B 7)) |
| $\Delta V$ | slip velocity ($\Delta V = V_g - V_l$) |
| $\Delta T$ | vapour subcooling ($\Delta T = T_s - T_g$) |
| $\tau_T$ | vapour thermal relaxation time (equation (3.11)) |
| $\tau_I$ | inertial relaxation time (equation (3.10)) |
| $\tau_{Tp}$ | thermal relaxation time in gas–particle mixture (equation (5.3)) |
| $\delta$ | ratio of specific heats ($\delta = c/c_{pg}$) |
| $\rho$ | density |

subscripts

| | |
|---|---|
| $\infty$ | unperturbed value at far upstream |
| d | dispersed phase (liquid droplets or solid particles) |
| e | equilibrium |
| f | frozen |
| g | vapour phase |
| l | liquid phase |

## References

Becker, E. 1970 Relaxation effects in gas dynamics. *Aeronaut. Jl R. Ae. S.* **74**, 736–748.

Crane, R. I. & Moore, M. J. 1972 Interpretation of pitot pressure in compressible two-phase flow. *J. Mech. Engng Sci.* **14**, 128–133.

Dussourd, J. L. & Shapiro, A. H. 1958 A deceleration probe for measuring stagnation pressure and velocity of a particle-laden gas stream. *Jet Propulsion* **28**, 24–34.

Guha, A. & Young, J. B. 1991 Time-marching prediction of unsteady condensation phenomena due to supercritical heat addition. *Proc. Conf. Turbomachinery: Latest Developments in a Changing Scene*, pp. 167–177. London, Institute of Mechanical Engineers.

Guha, A. 1992*a* Jump conditions across normal shock waves in pure vapour–droplet flows. *J. Fluid Mech.* **241**, 349–369.

Guha, A. 1992*b* Structure of partly dispersed normal shock waves in vapour–droplet flows. *Phys. Fluids* A **4**, 1566–1578.

Liepmann, H. W. & Roshko, A. 1957 *Elements of gasdynamics*, p. 105. New York: Wiley.

Marble, F. E. 1970 Dynamics of dusty gases. *A. Rev. Fluid Mech.* **2**, 397–446.

Petr, V. & Kolovratn'k, M. 1994 Laboratory and field measurements of droplet nucleation in expanding steam. *12th Int. Conf. on Properties of Water and Steam, Sept. 11–16.* FL, ASME.

Skillings, S. A. 1987 An analysis of the condensation phenomena occurring in wet steam turbines, p. 120. Ph.D. thesis, University of Birmingham, UK.

Skillings, S. A. 1989 Condensation phenomena in a turbine cascade. *J. Fluid Mech.* **200**, 409–424.

Stastny, M. & Sejna, M. 1994 Condensation effects in transonic flow through turbine cascade. *12th Int. Conf. on Properties of Water and Steam, Sept. 11–16.* FL, ASME.

Taylor, G. I. 1945 Pitot pressures in moist air. Reports and memoranda of the Aeronautical Research Council no. 2248.

White, A. J., Young, J. B. & Walters, P. T. 1996 Experimental validation of condensing flow theory for a stationary cascade of steam turbine blades. *Phil. Trans. R. Soc. Lond.* A **354**, 59–88.

Young, J. B. 1992 Two-dimensional, nonequilibrium wet steam calculations for nozzles and turbine cascades. *J. Turbomachinery Trans. ASME* **114**, 569–579.